

# MHD stability of ITER H-mode confinement with pedestal bootstrap current and diamagnetic effects taken into account

L. J. Zheng, M. T. Kotschenreuther, P. Valanju, S. Mahajan, D. Hatch and X. Liu

Institute for Fusion Studies, University of Texas at Austin, Austin, TX 78712, USA

*Corresponding Author:* lzheng@austin.utexas.edu

## Abstract:

The MHD stability of ITER H-mode confinement is investigated with bootstrap current included for equilibrium, together with the rotation and diamagnetic drift effects for stability. This is important because the ITER pedestal has high temperature, so that the bootstrap current and diamagnetic effects are large. We use the CORSICA code for computing the equilibrium and AEGIS for the stability. We find that the inclusion of bootstrap current for equilibrium calculation is critical. It can affect the MHD stability significantly. We find that the rotation can give rise to a stabilizing effect on RWMs. We also find that the diamagnetic drift effects can significantly reduce the RWM growthrate, but cannot fully eliminate the unstable RWMs. Only with the rotation effects included as well, the diamagnetic drift effects can further expand the stability parameter domain. Besides, we also investigate the effects of the safety factor value at the pedestal on MHD stability. We demonstrate that using the pedestal current ( $J_{ped}$ ) and pressure gradient ( $p'_{ped}$ ) alone is insufficient to draw an universal stability diagram. The safety factor value at the pedestal top, or the core plasma current, can also significantly affect the MHD stability conditions.

## 1 Introduction

The MHD stability of H-mode confinement [1] is critical to the success of ITER. It has been studied extensively in this field [2]. Note that the ITER pedestal has high temperature, so that the bootstrap current is large. In the earlier numerical reconstruction of tokamak equilibrium it is found that the bootstrap current can significantly modify the equilibrium safety factor profile, which is very important to MHD stability [3]. In our earlier work we shown that the MHD stability in JET can be significantly affected by such a change in the safety factor profile [4]. Also, since the pedestal pressure profile is steep and density is low near the edge, one can expect the diamagnetic effects to become important. These new physics concerns have motivated us to readdress the ITER MHD stability issue with the bootstrap current, plasma rotation, and diamagnetic effects taken into account.

In the equilibrium calculation we use the CORSICA code [5] to reconstruct ITER equilibrium, with the bootstrap current taken into account. We construct the free boundary equilibria and therefore the non-up-down symmetry feature is kept. In the stability

study we use the adaptive MHD stability code AEGIS [6], with rotation and diamagnetic effects included.

We investigate the  $n = 1$  resistive wall modes (RWMs) in ITER equilibrium, especially with the rotation and diamagnetic drift effects taken into account. It is found that both the rotation and diamagnetic drift can contribute stabilizing effects on the  $n = 1$  RWMs. We find that the diamagnetic drift stabilization effects can be enhanced by the rotation effects.

Besides, we note that the effects of the pedestal current ( $J_{ped}$ ) and pressure gradient ( $p'_{ped}$ ) on the MHD stability have been extensively exploited in this field. In this work we demonstrate that there are other parameters that can affect the MHD stability. Especially, we point out that the safety factor value at the pedestal top  $q_s$  is another factor to affect the system stability.

This manuscript is arranged as follows: In Sec. 2 the theoretical model and numerical scheme are described; In Sec. 3 the rotation and diamagnetic drift effects on the  $n = 1$  RWMs are studied; In Sec. 4 the effects of the safety factor value at the pedestal top  $q_s$  is examined. Conclusions and discussion are given in the last section.

## 2 Theoretical Model and Numerical Scheme

We focus on the ITER H-mode discharges. Due to the steep profiles in the narrow pedestal and the sensitivity of MHD stability to the quality of the MHD equilibria, very high-accuracy free-boundary equilibria are required (in which the safety factor  $q$  is calculated accurately because the Grad-Shafranov equation is satisfied to high accuracy at each point in the plasma up-to the region very near the separatrix). We calculate the necessary high accuracy MHD equilibria using the free-boundary CORSICA code [5] with ITER coils and plasma parameters. A large number (901) of radial points packed more in the pedestal region is adopted. A self-consistent loop is constructed in which the CORSICA equilibrium and the bootstrap current are iterated till convergence. The bootstrap current is calculated from the so-called Sauter model in Ref. [7]. This model has been favorably compared with other models in Ref. [8]. We then check the accuracy to which the Grad-Shafranov equation is satisfied at all plasma points. Resolving the edge  $q$  allows us to resolve the high  $m/n$  modes.

The plasma cross section is shown in Fig. 1. The conformal wall is used in our calculations. We include the bootstrap current in our equilibrium calculation. Typical pressure (here the ratio of plasma to magnetic energies  $\beta$  is used) and safety factor ( $q$ ) profiles are plotted in Fig. 2 and typical total parallel current density profile is given in Fig. 3. From Fig. 2 one can see that, taking into account the bootstrap current in

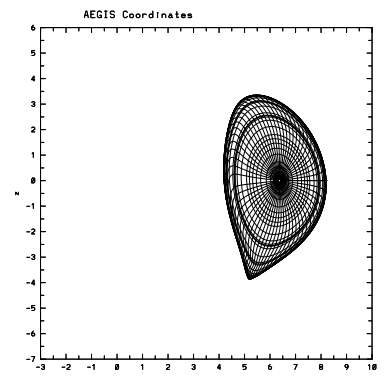


FIG. 1: ITER numerical equilibrium configuration, with grids packed on the rational surfaces by the AEGIS code.

the equilibrium calculation, a safety-factor reversal or plateau can indeed appear in the pedestal region. We denote the safety factor value at the region where the safety factor is flat or reversed as  $q_s$ .

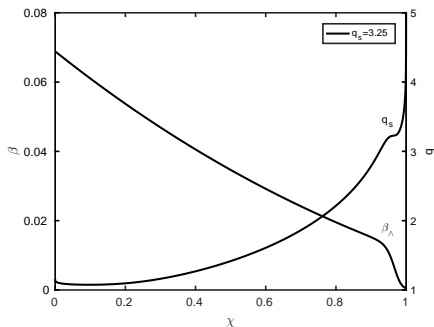


FIG. 2: Pressure ( $\beta$ ) and  $q$  profiles.

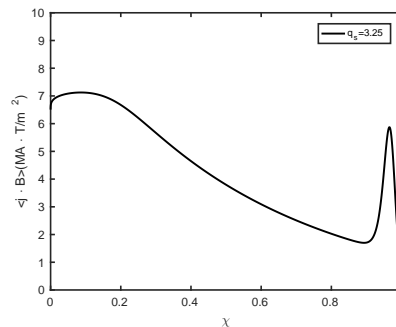


FIG. 3: Parallel current density profile.

In our stability study we include both the rotation and diamagnetic effects. We consider only the subsonic rotation case, i.e., the rotation frequency is assumed to be much lower than the ion acoustic frequency. In this case the rotational effects of centrifugal and Coriolis forces both on equilibrium and stability can be neglected [9, 10]. We then include the rotational effects only through the Doppler frequency shift in the stability analysis. To include the diamagnetic drift effects we apply the gyrokinetic theory given in Ref. [11]. Since we consider only the low frequency regime, we can exclude the wave-particle resonance effects. The sound wave coupling in this frequency regime contributes only to the so-called apparent mass effect [12]. The apparent mass effect is further enhanced by the so-called small parallel particle speed effect [13]. Nevertheless, we consider only the fluid apparent mass effect. As proved in Ref. [11], the finite Larmor radius effects are much more complicated after recovering the missing terms by the earlier gyrokinetic theories. However, if the steep pressure gradient in the pedestal is used as an auxiliary ordering, the finite Larmor radius effects are reduced dramatically to the sole modification of the mode frequency with the diamagnetic frequency shift:  $(\omega + n\Omega)^2 \rightarrow (\omega + n\Omega)(\omega + n\Omega - \omega_*)$ , where  $\omega$  is the mode frequency,  $\Omega$  is the toroidal rotation frequency, and  $\omega_*$  is the ion diamagnetic drift frequency.

In this case the basic set of equations become [11]

$$-\rho_m \hat{\omega}^2 \boldsymbol{\xi} = \delta \mathbf{J} \times \mathbf{B} + \mathbf{J} \times \delta \mathbf{B} - \nabla \delta P, \quad (1)$$

where

$$\hat{\omega}^2 = (\omega + n\Omega)(\omega + n\Omega - \omega_*),$$

$\boldsymbol{\xi}$  is the perpendicular field line displacement,  $\mathbf{B}$  denotes the equilibrium magnetic field,  $\delta \mathbf{B} = \nabla \times \boldsymbol{\xi} \times \mathbf{B}$  is the perturbed magnetic field,  $\mathbf{J}$  represents the equilibrium current density,  $\mu_0 \delta \mathbf{J} = \nabla \times \delta \mathbf{B}$  is the perturbed current density,  $\mu_0$  is the magnetic constant,  $P$  represents the equilibrium pressure,  $\delta P = -\boldsymbol{\xi} \cdot \nabla P$  is the perturbed pressure of convective

part, the perturbed quantities are tagged with  $\delta$  except  $\boldsymbol{\xi}$ , and  $\rho_m$  is the total mass, i.e., the sum of perpendicular mass and parallel mass (i.e., the apparent mass in the perpendicular momentum equation) [12]. We obtain Eq. (1) from the gyrokinetic theory. As pointed out in Ref. [11], equation (1) is consistent with Braginskii's two-fluid description.[14, 15] This diamagnetic drift modification in Eq. (1) can be viewed as keeping the finite Larmor radius effects in the lowest order in consideration of the pressure gradient steepness at the pedestal [15, 11]. Note that the adaptive numerical scheme of AEGIS code allows us to study the rotation-induced continuum damping [16].

Note that the inertia term on the left hand side of Eq. (1) can be regrouped using the formula:  $\hat{\omega}^2 = (\omega + n\Omega)(\omega + n\Omega - \omega_*) = (\omega + n\Omega - \omega_*/2)^2 - \omega_*^2/4$ . Subsequently, the quadratic form (i.e., the energy principle) can be formed from Eq. (1):

$$\delta W = \delta W_{mhd} + \delta W_{flr}, \quad (2)$$

where

$$\begin{aligned} \delta W &= \frac{1}{2} \int d\tau \rho_m (\omega + n\Omega - \omega_{*i}/2)^2 |\boldsymbol{\xi}|^2, \\ \delta W_{mhd} &= -\frac{1}{2} \int d\tau \boldsymbol{\xi}^\dagger \cdot [\delta \mathbf{J} \times \mathbf{B} + \mathbf{J} \times \delta \mathbf{B} - \nabla \delta P], \\ \delta W_{flr} &= \frac{1}{8} \int d\tau \rho_m \omega_*^2 |\boldsymbol{\xi}|^2. \end{aligned}$$

Here,  $d\tau$  is the volume element and the superscript  $\dagger$  represents the complex-conjugate. This regroup can help to understand the rotation and diamagnetic drift effects.

### 3 The Rotation and Diamagnetic Drift Effects on the Resistive Wall Modes

In this section we investigate the rotation and diamagnetic drift effects on the  $n = 1$  resistive wall modes. The equilibrium cross section and profiles are given in Figs. 1-3. The rotation frequency profile is assumed to be the same as the pressure profile.

First, we determine the critical wall position  $b_c$ . Here, the wall position ( $b$ ) is normalized by the minor radius at the mid-plane. The critical wall position is defined as follows: When the wall position is larger than  $b_c$ , the system is unstable with the perfectly conducting wall, otherwise stable. It is found that the critical wall position is  $b_c = 1.5$  for equilibrium given in Figs. 1-3.

We then calculate the  $n = 1$  resistive wall modes. The resistive wall modes only occur in the conducting wall stability regime, i.e.,  $b < b_c$ . The real and imaginary parts of the  $n = 1$  modes are given in Figs. 4 and 5 for  $b = 1.49$  without rotation and diamagnetic effects included. The growthrate is plotted by the solid curve in Fig. 6, as well as the subsequent figures in order to delineate the rotation and diamagnetic drift effects. Note here that, as is well-known, the RWM growthrate approaches infinity at the critical wall position.

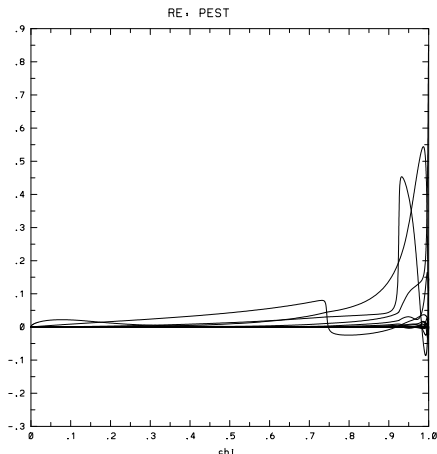


FIG. 4: Real part of the RWM eigenfunction.

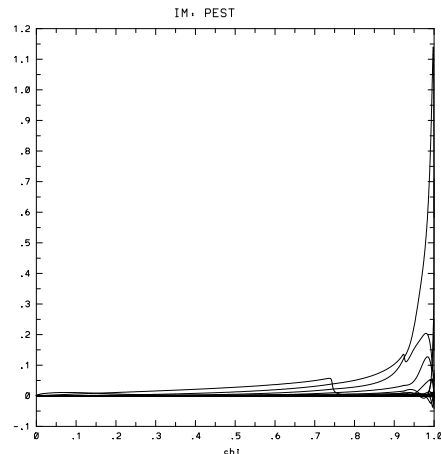


FIG. 5: Imaginary part of the RWM eigenfunction.

Next, we study the rotation effects. The results for rotation frequency  $\Omega = 0.03$  is given by the dashed curve in Fig. 6. From this figure one can see that rotation can stabilize RWMs near the critical wall position.

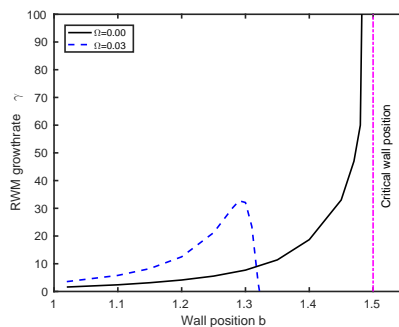


FIG. 6: The RWM growthrate vs the wall position with and without rotation.

Furthermore, we investigate the diamagnetic drift effects. The diamagnetic drift frequency profile is given in Fig. 7. Note that also due to the reduction of magnetic shear at the pedestal by the bootstrap current the modes accumulate near the edge as shown in Figs. 3 and 4. Since the diamagnetic drift frequency also peaks at the pedestal, one can expect the  $\omega_*$  stabilization for the modes to become significant. The RWM growthrate versus the wall position with and without the diamagnetic drift effects is plotted in Fig. 8. From this figure one can see that the diamagnetic drift reduces dramatically the RWM growthrate, especially near the critical wall position. Nevertheless, the diamagnetic drift alone cannot fully stabilize RWMs. The residual growing modes remain. This is because the RWM frequency approaches zero. The inertia effects are minimized in this case. With plasma rotation included, however, the diamagnetic drift effects are enhanced. The diamagnetic drift effects in the presence of rotation are also investigated. The results are plotted respectively in Figs. 9. From these this figure one can see that the diamagnetic

drift effects expand the stable regions.

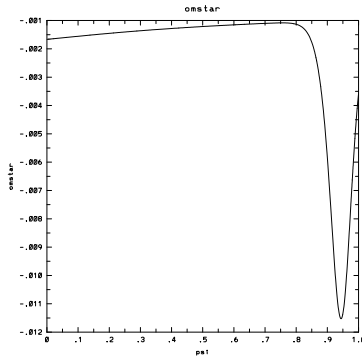


FIG. 7: The ion diamagnetic drift frequency profile.

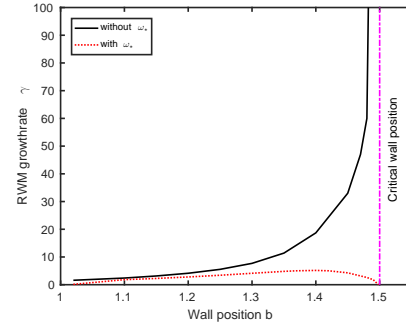


FIG. 8: The RWM growthrate vs the wall position with and without the diamagnetic drift effects.

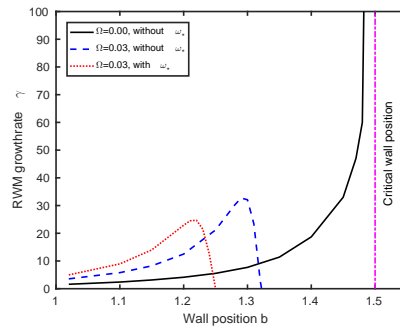


FIG. 9: The RWM growthrate vs the wall position with and without rotation and diamagnetic drift effects. The dotted curve corresponds to the inclusion of diamagnetic drift effects.

## 4 The Effects of the Safety Factor Value at the Pedestal

In this section we investigate the effects of the safety factor value at the pedestal. The effects of the pedestal current ( $J_{ped}$ ) and pressure gradient ( $p'_{ped}$ ) on the MHD stability are extensively exploited in this field. In this work we demonstrate that there are other effects can affect the MHD stability. Especially, we point out that the safety factor value at the pedestal top  $q_s$  is another factor to affect the system stability. Since the bootstrap current at the pedestal reduces the local magnetic shear, one can expect that the infernal mode branch resonating at  $q_s$  can also play a critical role. Consequently, the edge stability becomes to rely both on the peeling and infernal mode branches.

To prove the  $q_s$  effects we construct a series of equilibria with identical pressure profiles (see Fig. 10) and the pedestal current density profiles (see Fig. 11). The pedestal current

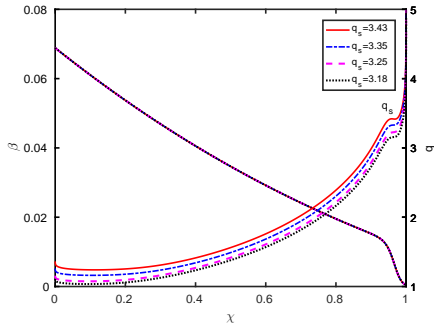
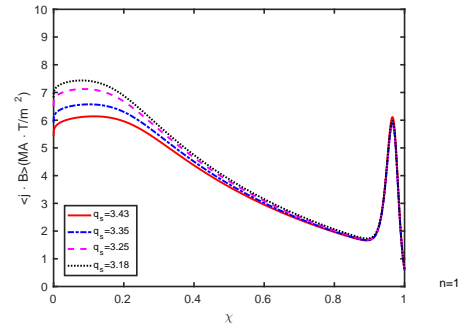
FIG. 10: Pressure and  $q$  profiles.

FIG. 11: Current density profiles.

$J_{ped}$  and pressure gradient  $p'_{ped}$  remain unchanged in this series of equilibria. The only change lies in the core plasma current as shown in Fig. 13. Consequently, the vertical shifts of safety factor profiles result and these equilibria have therefore different  $q_s$  values. The equilibrium corresponding to Figs. 2 and 3 investigated in the previous section corresponds to the case with  $q_s = 3.25$  in this series of equilibria. We compute the critical wall positions for  $n = 1 - 3$  ideal MHD external kink modes with perfectly conducting wall. The results are given in Table 1. From this table one can see that the critical wall position varies with the safety factor value  $q_s$  at the pedestal. This shows that using the pedestal current ( $J_{ped}$ ) and pressure gradient ( $p'_{ped}$ ) alone is insufficient to draw an universal stability diagram. The safety factor value at the pedestal top  $q_s$  needs to be taken into account as well.

Table 1: The critical wall position dependence on  $q_s$ 

$q_s$	$n = 1$	$n = 2$	$n = 3$
3.43	1.55	1.28	1.23
3.35	1.56	1.51	1.25
3.25	1.50	2.44	1.33
3.18	1.46	1.69	1.54

## 5 Conclusions and Discussion

In summary we have investigated the MHD stability of ITER H-mode confinement with the inclusions of bootstrap current for equilibrium and rotation and diamagnetic drift effects for stability using the CORSICA and AEGIS codes. We find that the inclusion of bootstrap current for equilibrium is critical. It can affect the MHD stability significantly.

We also investigate the rotation effects. We find that the rotation can give rise to a stabilizing effect on RWMs. The diamagnetic drift effects are also investigated in our work. We find that the diamagnetic drift effects can significantly reduce the RWM growthrate, but it alone cannot fully eliminate the unstable RWMs. Only with the rotation effects included as well, the diamagnetic drift effects can further extend the stability regime.

Besides, we also investigate the effects of the safety factor value at the pedestal by constructing a series of ITER equilibria with the pressure and pedestal current density profiles kept unchanged. We demonstrate that using the pedestal current ( $J_{ped}$ ) and pressure gradient ( $p'_{ped}$ ) alone is insufficient to draw an universal stability diagram. The safety factor value at the pedestal top, or the core plasma current, can also significantly affect the MHD stability conditions.

This research is supported by U. S. Department of Energy, Office of Fusion Energy Science.

## References

- [1] F. Wagner et al., Phys. Rev. Lett. **49**, 1408 (1982).
- [2] K. Ikeda, Nucl. Fusion **47** (2007).
- [3] C. E. Kessel et al., Nucl. Fusion **47**, 1274 (2007).
- [4] L. J. Zheng, M. T. Kotschenreuther and P. Valanju Nucl. Fusion **53**, 063009 (2013).
- [5] J.A. Crotinger et al, LLNL Report: UCRL-ID-126284,1997 NTIS #PB2005-102154.
- [6] L.-J. Zheng and M. Kotschenreuther, J. Comp. Phys. **211**, 748 (2006).
- [7] O. Sauter, C. Angioni, and Y. R. Lin-Liu, Phys. Plas. **6**, 2834 (1999).
- [8] M. C. R. Andrade and Go. O. Ludwig, Nucl Fus. **45**, 48 (2005).
- [9] F. L. Waelbroeck and L. Chen, Phys. Fluids B: Plasma Phys. **3**, 601 (1991) .
- [10] L.-J. Zheng, M. S. Chu, and L. Chen, Phys. Plasmas **6**, 1217 (1999).
- [11] L. J. Zheng, M. T. Kotschenreuther, and J. W. Van Dam, Phys. Plasmas **14**, 072505 (2007).
- [12] J. M. Greene and J. L. Johnson, Phys. Fluids **5**, 510 (1962).
- [13] L.-J. Zheng and M. Tessarotto, Phys. Plasmas **1**, 3928 (1994).
- [14] S. I . Braginskii, in Review of Plasma Physics, edited by M. A. Leontovich (Consultants Bureau, New York, 1965). Vol. 1, p. 205.
- [15] L.-J. Zheng, Phys. Fluids B: Plasma Phys. **5**, 1962 (1993).
- [16] L.-J. Zheng, M. Kotschenreuther, and M. S. Chu, Phys. Rev. Lett. **95**, 255003 (2005).